The anomalous and smoothed anomalous envelope spectra for rotating machine fault diagnosis

Stephan Schmidt[a,*], Konstantinos C. Gryllias[b,c]

[a] *Centre for Asset Integrity Management, Department of Mechanical and Aeronautical Engineering, University of Pretoria, Pretoria, South Africa*
[b] *Department of Mechanical Engineering, KU Leuven, Celestijnenlaan 300, 3001 Heverlee, Belgium*
[c] *Dynamics of Mechanical and Mechatronic Systems, Flanders Make, Belgium*

Abstract

The order-frequency spectral coherence and its integrated spectra (e.g. improved envelope spectrum, squared envelope spectrum) are some of the most powerful methods for performing fault diagnosis under time-varying operating conditions. However, it may require much work to interrogate the order-frequency spectral coherence for symptoms of damage. Hence, in this work we propose a methodology that combines the order-frequency spectral coherence with historical data that were acquired from a healthy machine to obtain an anomalous envelope spectrum, which is further processed for fault diagnosis. This anomalous envelope spectrum is further processed with a smoothing operation to not only perform automatic fault detection, but it is also possible to identify the damaged component if the kinematics of the gearbox are known. The proposed method is investigated on one numerical gearbox dataset and three experimental datasets, where its potential for performing automatic fault detection under time-varying operating conditions is highlighted.

Keywords:
Anomalous envelope spectrum, Cyclostationary analysis, Novelty detection, Blind fault detection, Time-varying operating conditions

1. Introduction

The vibration signals acquired from rotating machines are usually generated by periodic phenomena (e.g. gear mesh interactions, impacts due to bearing damage) [1]. As a result, the statistics of the signal are periodic in the angle domain and therefore the measured vibration signals can be described by the theory of cyclostationarity [1, 2]. This makes cyclostationary analysis techniques such as the squared envelope spectrum [3, 4], the instantaneous power spectrum [5, 6], the spectral correlation [7, 8] and the spectral coherence [7, 8] very powerful techniques for interrogating the vibration signals for symptoms of damage.

However, rotating machines such as wind turbines operate inherently under time-varying operating conditions [5, 9], which impedes the application of the conventional

*Corresponding author.
Email address: `stephan.schmidt@up.ac.za` (Stephan Schmidt)

time- or angle-based cyclostationary techniques [10]. This is attributed to the fact that even though the instantaneous power of the bearing damage component is periodic in the angle domain, the carrier of the signal is described by the dynamic properties of the structure, which are time-invariant [10]. Hence, neither the time nor angle domain representations are suited to describe these signals, and the signals should rather be described using angle-time cyclostationary theory [10]. Hence, the angle-frequency instantaneous power spectrum [5], the order-frequency spectral correlation [10] and Order-Frequency Spectral Coherence (OFSCoh) [10] should be used for analysing the vibration signals that were acquired under time-varying speed conditions.

The OFSCoh is currently one of the most powerful techniques for performing bearing diagnostics under time-varying operating conditions [10]. It is a bivariate representation of the cyclic orders of the angle-periodic modulation components and the spectral frequencies of their time-invariant carriers [10]. However, the two-dimensional representation can be difficult to interrogate when incipient damage is present and therefore the integrated spectral coherence is very useful for fault diagnosis [8, 11–13].

However, applying state-of-the-art signal analysis techniques can require much work to implement and much manual effort to investigate for symptoms of damage. In some cases the fault order of the component-of-interest needs to be specified a priori before the method can be applied e.g., [2, 12, 14]. This means that the techniques could be difficult to scale when many machines need to be monitored for damage. This has been one of the main motivations of developing deep learning fault diagnosis methods [15]; the methods make it possible to automatically determine the condition of the machine from the raw or processed vibration signals. Chen et al. [16] combined the spectral coherence and convolutional neural networks for automatic fault classification. However, many deep learning methods require much historical fault data to be available and the classification problem is actually an open set recognition problem (i.e. only historical fault data of some of the damage modes may be available), which could make it difficult to apply the supervised learning techniques in practice [17].

In Ref. [14], a methodology is proposed to combine the OFSCoh with healthy historical data. This is performed by firstly identifying the damage modes in the system and targeting their specific cyclic orders in the OFSCoh. Subsequently, a data-driven model was developed of the healthy behaviour of the features extracted from the targeted components, which was then used to automatically infer the health of the targeted components. However, if a complex drive train is under consideration, there may be many cyclic orders that need to be targeted to properly monitor the machine. It is also possible that the harmonics of the cyclic orders of different components can overlap, which may lead to ambiguous behaviour when performing inference.

Hence, in this work we propose a blind methodology that can be used for performing fault diagnosis under time-varying operating conditions. The outcome of this methodology is the Anomalous Envelope Spectrum (AES) and the smoothed AES (sAES), which are calculated by combining the OFSCoh and historical data from a healthy machine. The AES is a powerful representation that can be used to detect faults and it can also help to identify which components are damaged. It has the additional benefit, compared to Ref. [14] for example, that it does not require the components-of-interest to be known nor specified before applying the methodology, i.e. it is blind. It is only desirable to know the kinematics of the gearbox if the AES is interrogated to determine which machine component is damaged.

In summary, the contributions of this paper are the following:

- A new representation, the Anomalous Envelope Spectrum (AES), is proposed which can be processed to perform fault diagnosis under time-varying operating conditions. We propose using a smoothing operation between consecutive OFSCohs before the AES is calculated. This processed AES is referred to as the smoothed AES (sAES) in this work.
- This method is simple to implement and scalable for monitoring many machines. This is because historical data are used to supplement the OFSCoh for fault detection and identification under time-varying operating conditions, i.e. it is not necessary to manually interrogate the signals.

The layout of the paper is as follows: In Section 2, an overview of the proposed method is given, whereafter the method is applied on numerical gearbox data in Section 3 and on three experimental gearbox datasets in Section 4. Finally, the paper is concluded in Section 5. Appendix A contains additional information pertaining to the threshold selection discussed in Section 2; Appendix B contains additional information of the numerical gearbox model presented in Section 3; and Appendix C contains additional results obtained on the experimental data discussed in Section 4.

2. Proposed methodology

We desire to develop a vibration-based condition monitoring methodology that enables us to determine the condition of the machine at time step i, without requiring the cyclic orders of interest to be specified beforehand, i.e. the methodology is blind. This methodology is developed under the following assumptions:

- There are much historical data available that describe the behaviour of the machine in a reference condition, whereafter the machine is monitored for damage.
- An accurate estimate of the rotational speed is available at each measurement, with the rotational speed at time step i denoted by $\omega^{(i)}(t)$. If the speed cannot be measured, it is possible to use a tacholess speed estimation method [18, 19] before applying this methodology.
- Regular measurements are taken during the condition monitoring process. The vibration signal acquired at time step i is denoted by $x^{(i)}(t)$ and its corresponding sampling frequency is f_s.

2.1. Preliminary theory

The Order-Frequency Spectral Coherence (OFSCoh) can highlight weak damage components in the signal and therefore enables incipient damage to be detected [10, 11]. The OFSCoh of the vibration measurement acquired at time step i [10]

$$\gamma^{(i)}(\alpha, f) = \frac{S_{xx}^{(i)}(\alpha, f)}{\left| S_x^{(i)}(0, f) \cdot S_{x_\alpha}^{(i)}(0, f) \right|^{1/2}}, \tag{1}$$

is calculated with the order-frequency spectral correlation $S_{xx}^{(i)}(\alpha, f)$, the power spectral density of the vibration signal $x^{(i)}(t)$ denoted by $S_x^{(i)}(0, f)$ and the power spectral density of $x_\alpha^{(i)}(t) = x^{(i)}(t) \cdot e^{-j\alpha\theta^{(i)}(t)} \cdot \omega^{(i)}(t)$ denoted by $S_{x_\alpha}^{(i)}(0, f)$ [10]. The imaginary unit is denoted by $j = \sqrt{-1}$. In Equation (1), α denotes the cyclic order variable and f denotes the spectral frequency variable. The order-frequency spectral correlation is calculated with [10]

$$S_{xx}^{(i)}(\alpha, f) = \lim_{W \to \infty} \frac{1}{\Phi(W)} \mathbb{E} \left\{ \mathcal{F}_W(x^{(i)}(t))^* \cdot \mathcal{F}_W \left(x^{(i)}(t) \cdot e^{-j\alpha\theta^{(i)}(t)} \cdot \omega^{(i)}(t) \right) \right\}, \tag{2}$$

where $\mathcal{F}_W(\cdot)$ is the Fourier transform over a time length of W, $x^{(i)}(t)$ is the measurement taken at time step i, $\omega^{(i)}(t)$ is the corresponding instantaneous rotational speed of a shaft and $\theta^{(i)}(t)$ is the corresponding instantaneous phase of the shaft. The cumulative phase of the shaft after a time duration of W is denoted $\Phi(W)$. The reason why the measurement index i is emphasised in all of the terms, is because this is important for the calculation of the processed AES and it ensures that a consistent notation is used. The order-frequency spectral correlation is estimated with the Welch-based estimator proposed in Ref. [10], due to its good bias and variance properties. However, much faster estimators of the spectral correlation can be used if desired [11, 20].

The integrated spectral coherence is very useful for gearbox diagnostics, due to the fact that it is simpler to interrogate for damage than the bivariate OFSCoh [12, 13]. The Squared Envelope Spectrum is the most popular signal analysis technique for performing bearing fault diagnosis [4] and can be estimated from the OFSCoh with [11, 13, 21]

$$\mathrm{SES}^{(i)}(\alpha) = \left| \int_0^{f_s/2} \gamma^{(i)}(\alpha, f) df \right|, \tag{3}$$

for the ith signal, while the enhanced envelope spectrum can be estimated with

$$\mathrm{EES}^{(i)}(\alpha) = \int_0^{f_s/2} \left| \gamma^{(i)}(\alpha, f) \right|^2 df. \tag{4}$$

The sampling frequency of the signal is denoted by f_s. It was shown in Ref. [11] that in general the EES is better suited for incipient fault detection than the SES. Hence, it is possible to estimate the SES and the EES with Equations (3) and (4) without performing bandpass filtering on the raw vibration signal.

It is possible to improve the signal-to-noise ratio of the damaged components in the integrated spectrum by limiting the integration band of the SES and the EES to a band $[f_l, f_h]$. This is because the impulses generated by damaged components excite resonances in the system, which means that the fault information manifests in narrow frequency bands [22]. The integration of the OFSCoh over the band $[f_l, f_h]$ is used to define the Improved Envelope Spectrum (IES) [11],

$$\mathrm{IES}^{(i)}(\alpha; f_l, f_h) = \int_{f_l}^{f_h} \left| \gamma^{(i)}(\alpha, f) \right|^2 df, \tag{5}$$

where $0 < f_l < f_h$ and $f_h < f_s/2$. Therefore, if the integration band $[f_l, f_h]$ is carefully selected, the IES can improve the signal-to-noise ratio of the fault information. However, selecting the appropriate frequency band automatically can be difficult to perform, especially if the fault information is weak. This has resulted in the development of the IESFOgram, which aims to detect the frequency band that is optimal for detecting specific targeted signal components [23]. Even though the IESFOgram performs very well in identifying the optimal integration band, it requires the targeted cyclic orders to be specified a priori. This can be difficult when complicated drive-trains with many fault orders need to be monitored or when the fault orders are not known.

The proposed methodology was developed to allow us to automatically identify the frequency bands that have important information and then to use this to obtain an intuitive representation for fault diagnosis. The Anomalous Envelope Spectrum (AES) is presented in the next section.

2.2. Anomalous Envelope Spectrum (AES)

The AES is derived from the Generalised Integrated Spectrum (GIS) in this work. The GIS of the ith vibration measurement is obtained from the integrated spectrum of the OFSCoh by including a general weighting function $\mathcal{G}(\alpha, f)$

$$\mathrm{GIS}^{(i)}(\alpha) = \int_0^{f_s/2} \left|\gamma^{(i)}(\alpha, f)\right|^2 \cdot \mathcal{G}(\alpha, f)\, df, \tag{6}$$

where the weighting function $0 \leq \mathcal{G}(\alpha, f) \leq 1$. This GIS has the following properties:

- The EES is obtained by setting $\mathcal{G}(\alpha, f) = 1\ \forall\ f \in [0, f_s/2]$, i.e. then $\mathrm{GIS}^{(i)}(\alpha) = \mathrm{EES}^{(i)}(\alpha)$.
- The IES is obtained by setting $\mathcal{G}(\alpha, f) = 1\ \forall\ f \in [f_l, f_h]$ and $\mathcal{G}(\alpha, f) = 0\ \forall\ f \notin [f_l, f_h]$, i.e. then $\mathrm{GIS}^{(i)}(\alpha) = \mathrm{IES}^{(i)}(\alpha; f_l, f_h)$.

Since it is assumed that healthy historical data are available, it is possible to construct a function $G(\alpha, f)$ to automatically highlight regions in the OFSCoh that have non-healthy (i.e. anomalous) behaviour. This anomaly function $G(\alpha, f)$ indicates whether healthy ($G(\alpha, f) = 0$) or anomalous ($G(\alpha, f) = 1$) behaviour is seen at a cyclic order α and a spectral frequency f in $|\gamma^{(i)}(\alpha, f)|^2$. If we use this anomaly function $G(\alpha, f)$ in the GIS, the Anomalous Envelope Spectrum (AES)

$$\mathrm{AES}^{(i)}(\alpha) = \int_0^{f_s/2} \left|\gamma^{(i)}(\alpha, f)\right|^2 \cdot G(\alpha, f)\, df, \tag{7}$$

is obtained. The AES is used to identify components that are anomalous (e.g. attributed to machine damage or spurious noise). Hence, as opposed to selecting or estimating the optimal f_l and f_h to determine the IES with the GIS, only the information from anomalous frequency bands are retained in the AES.

2.3. Estimation of the AES

The OFSCohs associated with the N_h measurements from a healthy machine, denoted by $\{\gamma_h^{(i)}(\alpha, f)\}_{i \in \mathbb{Z}, 0 \leq i \leq N_h - 1}$, are used to calculate a threshold $\tau(\alpha, f)$. This threshold is used to automatically determine whether a specific combination of cyclic orders and spectral frequencies of the ith measurement contain anomalous information $\left|\gamma^{(i)}(\alpha, f)\right|^2 > \tau(\alpha, f)$

or not $\left|\gamma^{(i)}(\alpha,f)\right|^2 \leq \tau(\alpha,f)$. This is used to define the anomaly function G for the measurement at time step i as follows:

$$G^{(i)}(\alpha,f) = \begin{cases} 1 & \text{if} \quad |\gamma^{(i)}(\alpha,f)|^2 > \tau(\alpha,f) \\ 0 & \text{if} \quad |\gamma^{(i)}(\alpha,f)|^2 \leq \tau(\alpha,f). \end{cases} \tag{8}$$

It is possible to use kernel density estimators to detect anomalous behaviour with the spectral coherence as investigated in Ref. [14], however, this can be computationally intensive to use and it is required to find the optimal hyperparameters for each combination of α and f. If it is assumed that the data are Gaussian, the threshold can be defined by:

$$\tau(\alpha,f) = \mu_\gamma(\alpha,f) + \kappa \cdot \sigma_\gamma(\alpha,f), \tag{9}$$

where κ is a factor, $\mu_\gamma(\alpha,f)$ is the mean and $\sigma_\gamma(\alpha,f)$ is the standard deviation of the healthy spectral coherences. However, the sampling distribution of the spectral coherence is not expected to be Gaussian. In Ref. [7], it was shown that the spectral coherence has a chi-square distribution when long signals are considered. Using the empirical distribution of the data to set the threshold is another approach that can be used. For example, the inter-percentile range can be used to obtain a threshold with

$$\tau(\alpha,f) = \kappa \cdot (p_\xi(\alpha,f) - p_{100-\xi}(\alpha,f)) + p_{100-\xi}(\alpha,f), \tag{10}$$

where $p_\xi(\alpha,f)$ is the ξth percentile of the set of healthy spectral coherences, denoted by $\{\gamma_h^{(i)}(\alpha,f)\}$, at a specific cyclic order α and spectral frequency f. A special case of this range is the interquartile range where $\xi = 75$. If $\kappa = 1$, it means that the ξth percentile is used for detecting outliers, which could result in false alarms. In addition to this, the threshold in Equation (10) is estimated from limited healthy measurements and is therefore a random variable. Hence, it is therefore suggested that $\kappa > 1$. In a practical situation, it would be better to use different κs to obtain a range of thresholds for decision making, e.g. one threshold can act as a warning and another threshold can automatically stop the machine. The interpretation and use of the threshold would depend on the machine and its application (e.g. implications of a sudden failure).

The OFSCoh is estimated from a finite length signal and since the OFSCoh is sensitive to weak components in the signal, it could contain spurious noise. This would result in the anomaly function $G^{(i)}(\alpha,f)$ to indicate anomalous behaviour, i.e. $G^{(i)}(\alpha,f) = 1$, for healthy cyclic orders and spectral frequencies. The robustness of the AES can be increased by utilising the information from consecutive measurements to obtain the smoothed AES (sAES), which is a more robust representation of the condition of the gearbox under consideration. The smoothed AES (sAES) is calculated with

$$\text{sAES}^{(i)}(\alpha) = \int_0^{f_s/2} \mathcal{P}\left\{|\gamma^{(m)}(\alpha,f)|^2 \cdot G^{(m)}(\alpha,f)\right\}_{m\in\mathbb{Z}, i-N_s \leq m \leq i} df, \tag{11}$$

where N_s is the number of consecutive measurements that is used for processing the weighted spectral coherences $|\gamma^{(m)}(\alpha,f)|^2 \cdot G^{(m)}(\alpha,f)$. We refer to this AES as the smoothed AES so that it is not confused with the raw AES obtained with Equation (7). The smoothing function $\mathcal{P}$ can for example be the median or the mean. If the

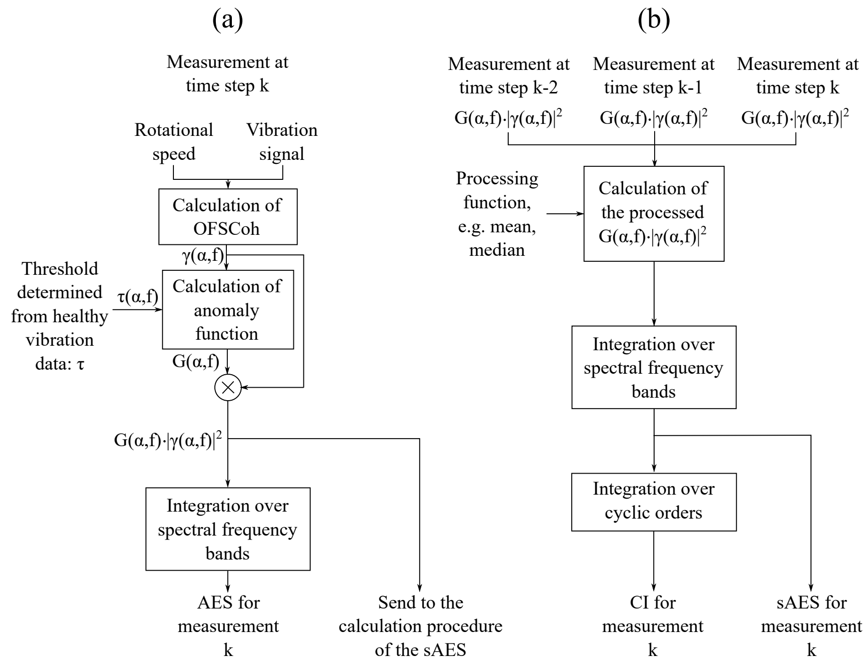

Figure 1: The calculation procedure of the Anomalous Envelope Spectrum (AES) for measurement k is shown in (a), while the calculation procedure of the smoothed AES (sAES) and its corresponding Condition Indicator (CI) are shown at time step k by using the information from the previous 3 time steps, i.e. $N_s = 3$ in Equation (11).

mean is used, the integrated spectrum of the moving averaged OFSCoh, i.e. the average of $|\gamma^{(m)}(\alpha, f)|^2 \cdot G^{(m)}(\alpha, f)$ is calculated over measurement index m. The sAES can subsequently be used for automatic fault detection by searching for cyclic orders where $\text{sAES}^{(i)}(\alpha) > 0$ and if the kinematics of the drive train are known, it would also be possible to identify the damaged component.

Lastly, the sAES can be used to obtain a Condition Indicator (CI) for time step i as follows:

$$\text{CI}_i = \frac{1}{\alpha_{max}} \int_0^{\alpha_{max}} \text{sAES}^{(i)}(\alpha)\, d\alpha, \tag{12}$$

with $\text{CI}_i > 0$ indicates that anomalous behaviour is present, while $\text{CI}_i = 0$ indicates that the spectral coherence of the measurement at time step i displays healthy behaviour. Since the smoothing operation removes the spurious anomalous components, the threshold can be set to $\text{CI}_i = 0$ for detecting anomalous behaviour. This threshold was used in subsequent sections. It is also possible to investigate other blind features such as the L2/L1 ratio [24] or the spectral negentropy [25] of the AES, but the optimisation of the condition indicator and the threshold selection is not considered in this work.

2.4. Summary

The calculation procedures of the AES and the sAES that were described in the previous sections are summarised in Figures 1(a) and 1(b) for time step k. The following parameters are used in all investigations:

- The median is used as the processing function $\mathcal{P}$ in Equation (11). The median is much more robust to outliers than the mean and can therefore provide a more reliable estimate of the actual condition of the machine.

- The number of measurements used in calculating the sAES, i.e. N_s in Equation (11), is set to $N_s = 10$.
- The percentile ϵ and the factor κ in Equation (10) are set to $\epsilon = 95$ and $\kappa = 4$, respectively. The 95 percentile is used, because it is assumed that the healthy dataset does not contain much outliers and we desire to utilise the full distribution for detecting outliers in the damaged signal. We have found that $\kappa = 4$ ensures that the method is not too sensitive to outliers attributed to noise in the data and can therefore result in less false alarms, while still performing very well in fault detection and fault trending. The κ is further motivated in Section 4.2 and Appendix A.

This method is firstly investigated on numerical gearbox data in the next section, whereafter the method is investigated on three experimental gearbox datasets in Section 4.

3. Numerical gearbox investigation

The phenomenological gearbox model presented in Ref. [4] is considered in this work to simulate vibration data acquired from a gearbox operating under time-varying speed conditions. The measured casing vibration signal of the gearbox in its reference condition

$$x_c(t) = x_{gmc}(t) + x_{dgd}(t) + x_n(t), \tag{13}$$

is decomposed in terms of three components, namely, a deterministic gear mesh component denoted $x_{gmc}(t)$, a random gear component attributed to distributed gear damage denoted by $x_{dgd}(t)$ and a broadband noise component denoted by $x_n(t)$. Forty measurements were taken from the gearbox in its reference condition, whereafter an additional signal component due to outer race bearing damage is added to the casing vibration signal. The new casing vibration signal

$$x_c(t) = x_{gmc}(t) + x_b(t) + x_{dgd}(t) + x_n(t), \tag{14}$$

contains the additional bearing damage component denoted $x_b(t)$. More information regarding the signal components is given in Appendix B. Two-hundred measurements from the damaged gearbox are investigated in this section, with the magnitude of the bearing component increasing monotonically with the measurement number as discussed in Appendix B and shown in Figure B.18.

The time-varying rotational speed profiles that were used to generate the vibration data are presented in Figure 2(i). The casing vibration signal of the 110th measurement from the damaged gearbox (i.e. Equation (14)) shown in Figure 2(ii) is used to illustrate the different steps of the proposed method in this section.

The OFSCoh of the damaged gearbox is presented in Figure 3(i) for the measurement considered in Figure 2(ii). In Figure 3(i), the distributed gear damage component is clearly seen at a spectral frequency of 1.3 kHz and the components associated with the bearing damage are seen at 7 kHz. The methodology was applied on the 110th measurement of the considered dataset to obtain the resulting weighted OFSCoh, which is presented in Figure 3(ii). The weighted OFSCoh, calculated with $G^{(i)}(\alpha, f) \cdot |\gamma^{(i)}(\alpha, f)|^2$, only contains the bearing component at the spectral frequency of 7kHz, because the bearing damage component is the only novel component in the signal. Hence, the weighted OFSCoh is able

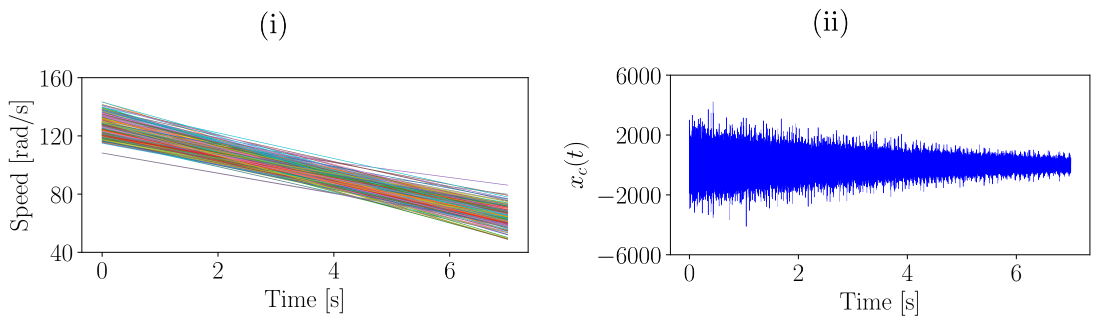

Figure 2: The rotational speeds that are under consideration in the phenomenological gearbox data as well as the vibration signal corresponding to the 110th measurement of the damaged gearbox.

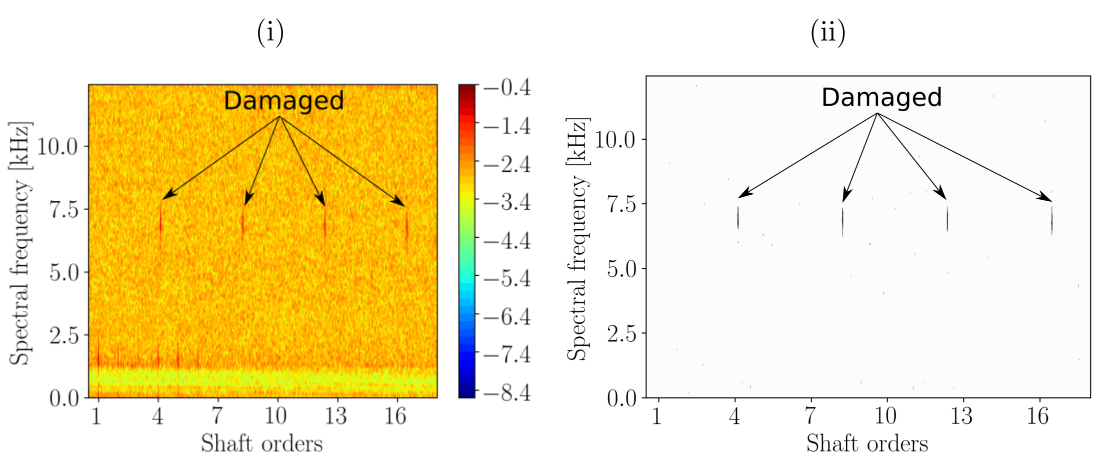

Figure 3: The OFSCoh of the vibration signal is presented in Figure 3(i) for the 110th measurement in the damaged dataset. The corresponding weighted OFSCoh is presented in Figure 3(ii).

to enhance the novel components in the signal and attenuate the dominant components that were in the reference signal.

The integrated spectra, i.e. the EES, the AES and the sAES, are presented in Figure 4 for two measurements. No additional processing was performed before the EES and AES were calculated. The distributed gear damage component, with a cyclic order of 1.0 shaft orders, is dominant in the OFSCoh and therefore makes the weak bearing damage components more difficult to detect in the EES shown in Figure 4. Since both signals are random, they cannot be separated using techniques such as the generalised synchronous average [4]. In contrast to the EES, the bearing damage components are very prominent in the AES and the sAES, since the distributed gear damage components are removed in the weighted OFSCoh presented in Figure 3(ii). The sAES contains much less noise than the AES due to the additional processing that is performed.

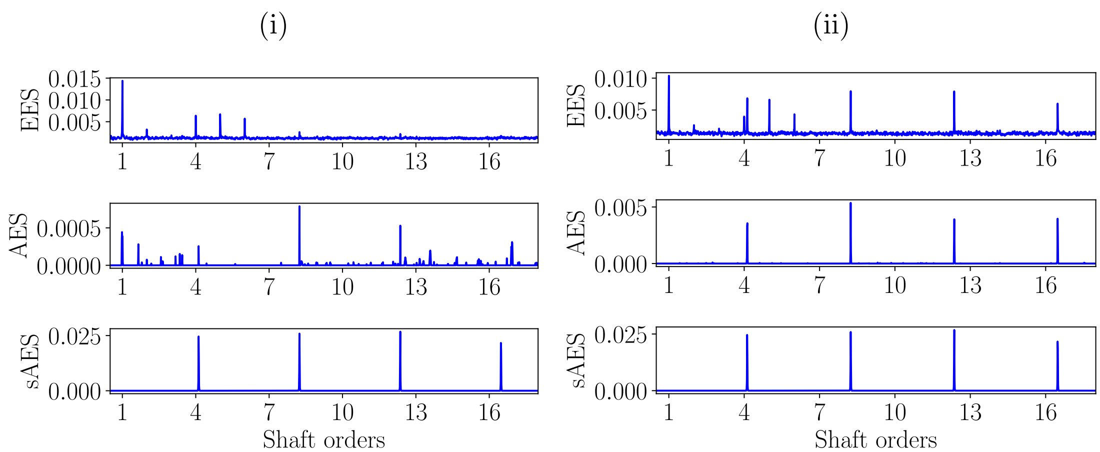

Figure 4: The integrated spectra are presented for two measurements in the damaged gearbox dataset. The integrated spectra of the 77th measurement and 110th measurement are presented in Figures 4(i) and 4(ii) respectively.

Since it is not only important to determine whether it is possible to detect bearing damage, but also whether changes in the condition can be detected, different magnitudes of bearing impulses are investigated. The magnitude of the bearing impulses were increased monotonically over the measurement number. Please refer to Figure B.18 for more information. The EES and the sAES of the different measurements under consideration are presented in Figures 5(i) and 5(ii), respectively. The exact signal-to-noise ratios of the bearing component for each measurement are included in Appendix B. The distributed gear damage and bearing damage components can be seen in the EES presented in Figure 5(i), while the sAES does not contain any signal components until the bearing damage component is detected. The bearing damage components at 4.12 shaft orders and its harmonics are clearly seen.

The mean of the integrated spectra are investigated as condition indicators for fault trending. The mean of the EES and the mean of the sAES as calculated with Equation (12) are presented in Figures 5(iii) and 5(iv) respectively. The condition indicator of the EES contains much noise which makes it difficult to observe the increase of the condition indicator due to the change in the magnitude of the bearing component. However, the CI

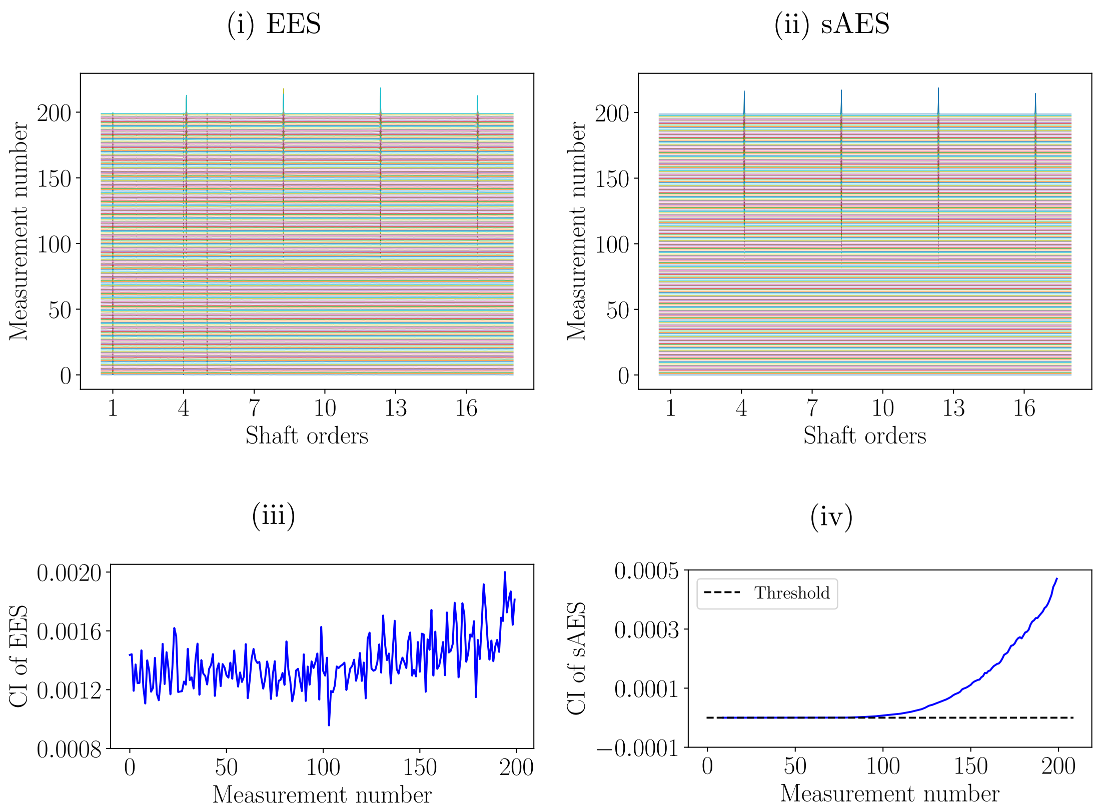

Figure 5: A waterfall plot of the EES and the sAES as well as their corresponding condition indicators are presented for the phenomenological gearbox model.

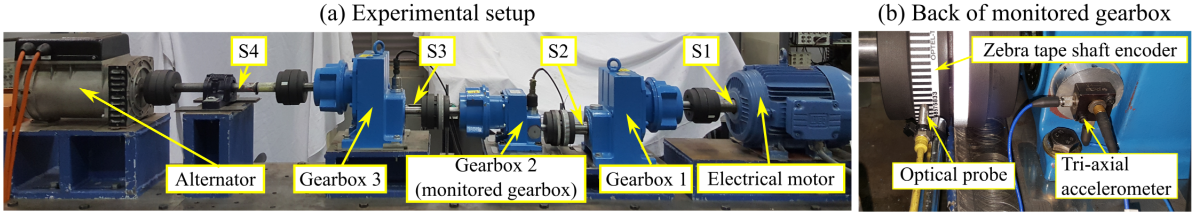

Figure 6: The experimental setup with the important components and parts highlighted.

of the sAES performs much better, due to the fact that it is not affected by the noise in the signal and provides a monotonic trend which is consistent with the magnitude of the bearing impulses that increases monotonically over the measurement number.

Hence, the proposed anomalous envelope spectrum and its related metrics are not only capable of detecting changes in the condition of the bearing, but it is also able to identify at which cyclic orders the damage manifests when inspecting the sAES. In the next section, the proposed method is investigated on experimental data.

4. Experimental gearbox investigation

The proposed method is now investigated on experimental data that were acquired from a helical gearbox under time-varying operating conditions. In Section 4.1, an overview of the experimental setups and the measurement equipment is given, whereafter measurements taken from a gearbox with localised gear damage are investigated in Section 4.2 and measurements taken from a gearbox with distributed gear damage are investigated in Section 4.3. Finally, the method is investigated on healthy gearbox data in Section 4.4.

4.1. Experimental setup

The data considered in this section were acquired from the experimental setup shown in Figure 6. The experimental setup consists of three helical gearboxes, an alternator and an electrical motor. The shafts between the different components are denoted by S1, S2, S3 and S4 respectively. The centre helical gearbox is monitored for damage with two accelerometers, namely, a single-axis accelerometer and a tri-axial accelerometer. The methodology is applied on the axial-component of the tri-axial accelerometer, which is located on the bearing housing of the monitored gearbox as seen in Figure 6(b). The instantaneous speed of the input shaft of the gearbox (i.e. S2 in Figure 6) was measured with the optical probe and the zebra tape shaft encoder also shown in Figure 6(b). An OROS OR 35 data acquisition device was used with an accelerometer signal that was sampled at a rate of 25.6 kHz, while the optical probe was sampled at 51.2 kHz.

The electrical motor and the alternator were independently controlled to apply the time-varying operating conditions to the monitored gearbox as shown in Figure 7.

The monitored helical gearbox in Figure 6 consists of a gear and a pinion. The pinion was kept healthy for all measurements, while the gear was damaged as discussed in the next sections. Since the gear is connected to the reference shaft S2 in Figure 6, it rotates at 1.0 shaft order. This means that impacts from a damaged gear tooth would modulate the signal at 1.0 shaft order and would therefore be detected at 1.0 shaft order and its harmonics when interrogating the envelope spectrum. In Appendix C, the RMS, the

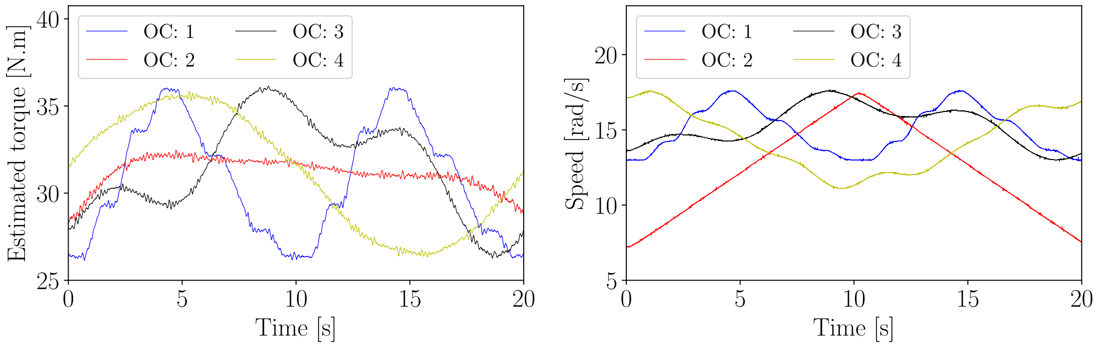

Figure 7: The operating conditions that were estimated at the input shaft of the gearbox, i.e. $S2$ in Figure 6.

(i) Before (ii) After

Figure 8: The gear with localised gear damage is presented. In Figure 8(i), the gear before the fatigue experiment is presented, while in Figure 8(ii) the gear after the fatigue experiment is presented.

kurtosis and the L2/L1-norm ratio of the SES are presented for the raw vibration signals considered in this work. This is to further highlight the benefits of using the proposed method.

4.2. Localised gear damage experiment

Localised gear damage such as root cracks can severely affect the remaining useful life of gearboxes and is therefore very important to detect. An experiment was firstly performed with both gears of the monitored gearbox being healthy. Forty measurements, taken while the gearbox was operating under operating condition 1 in Figure 7, are used to calculate the bivariate threshold function $\tau(\alpha, f)$ with Equation (10). Thereafter, the gearbox was disassembled and the gear was damaged by seeding a small slot in the root of the gear tooth as shown in Figure 8(i). The helical gears have much larger contact ratios than spur gears, which makes the gear damage shown in Figure 8(i) more difficult to detect. The monitored gearbox was reassembled with the damaged gear and tested for approximately 20 days under operating condition 1 before the damaged tooth failed as shown in Figure 8(ii). Two-hundred measurements, approximately evenly spaced over the testing period, are used to evaluate the effectiveness of this methodology.

However, this experiment does not represent the actual conditions that would be expected in a real application. If maintenance is performed on the system, the damaged

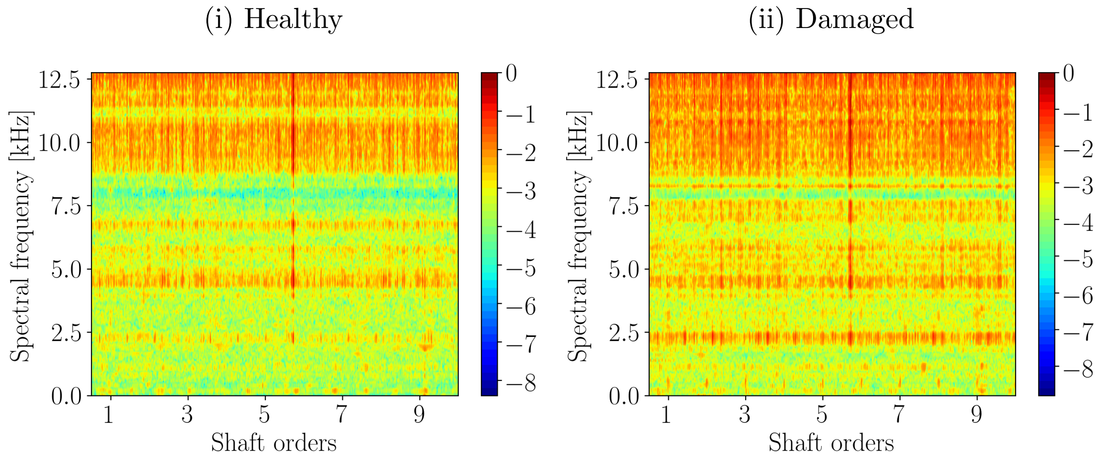

Figure 9: The logarithm of the mean OFSCoh of the healthy data and the logarithm of the OFSCoh from a damaged signal are presented in Figures 9(i) and 9(ii) on different colour scales.

components would be replaced with healthy components, which would make new measurements available for calculating the threshold τ. In this experiment, we needed to replace the gear with a damaged gear to ensure that the gear would fail in a reasonable time. The implication of this is that there may be some differences between the experimental setup under consideration and the reference experimental setup which could also result in the measurements to have different statistical properties. Hence, κ in Equation (10) was made sufficiently large to ensure that false alarms are avoided.

The average spectral coherences of the healthy measurements are presented in Figure 9(i) to emphasise the motivation of using a bivariate threshold $\tau(\alpha, f)$ in the method. If the threshold was set to a constant value for all cyclic orders and spectral frequencies, it may be too sensitive to noise at specific combinations of α and f, while being insensitive to damage at other combinations of α and f.

The OFSCoh of one of the measurements from the damaged gearbox is presented in Figure 9(ii). The damaged components are located in a resonance band at approximately 500 Hz, but the OFSCoh is dominated by other phenomena which make the damage difficult to detect. The corresponding weighted OFSCoh is presented in Figure 10(i). Since the impacts attributed to localised gear damage are the only new information in the signal, the weighted OFSCoh retains only the damaged information in the aforementioned frequency bands as seen in Figure 10(i). Since the damage only manifest in a very localised region of the OFSCoh, a zoomed view is included in Figure 10(i). Lastly, the different integrated OFSCoh of the measurement from the damaged gearbox are presented in Figure 10(ii). The EES only retains a strong component at 5.72 shaft orders, but the components attributed to the gear damage cannot be clearly seen. The AES and the sAES perform much better, because they are able to identify the damaged components in the signal, with the sAES containing a much clearer representation due to the additional processing that is performed. Hence, it is clear that the proposed method is a very powerful representation for identifying frequency bands with novel information and using this not only for fault detection, but also for fault identification.

The EES and the sAES are presented over the measurement number in Figure 11. The

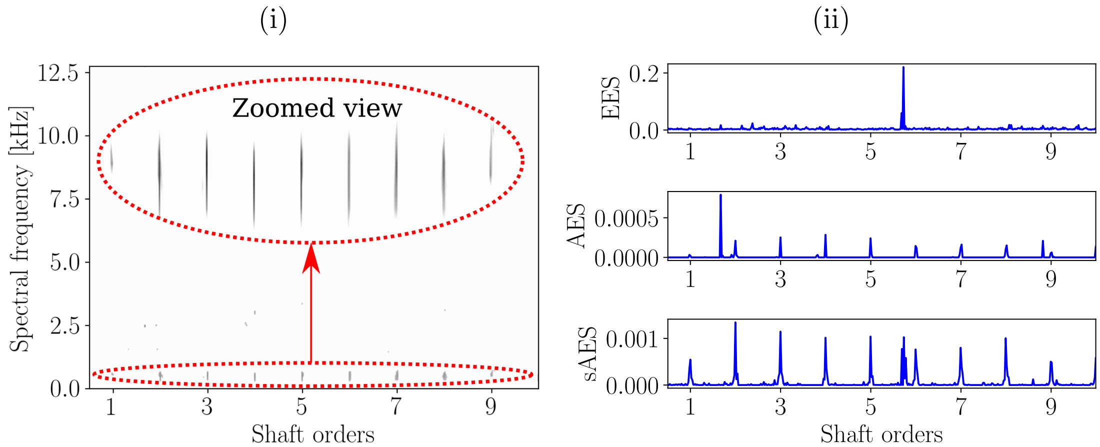

Figure 10: The weighted OFSCoh and corresponding integrated spectra are presented for the same signal considered in Figure 9(ii).

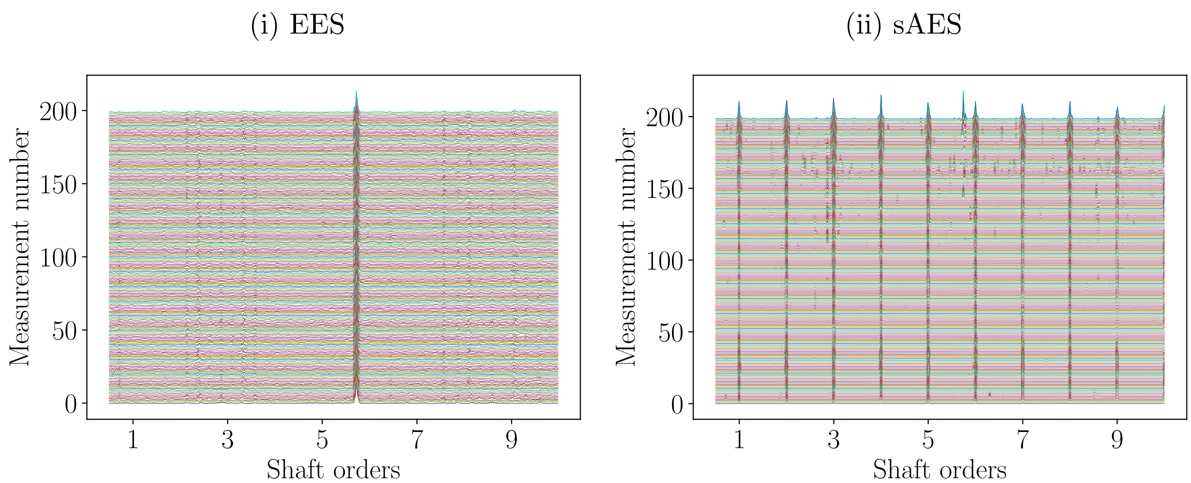

Figure 11: The Enhanced Envelope Spectra (EES) and the smoothed Anomalous Envelope Spectrum (sAES) of the data acquired from the gearbox with localised gear damage.

EES contains the very strong component at 5.72 shaft orders for all measurements, while being unable to detect the damaged gear component. This dominant signal component is present in both the healthy and the damaged datasets, however, it impedes the detection of the damaged gear component. The signal component at 5.72 shaft orders is attributed to the movement of the floating shaft in the monitored gearbox that results in undesired contact between the bearing and the casing of the gearbox. The movement is exacerbated by the fact that the input shaft of the helical gearbox has strong axial excitations due to the axial forces of the helical gears.

In contrast, the sAES performs much better than the EES. In the sAES in Figure 11, the signal components associated with the damaged gear are very prominent in the spectrum, while it is also possible to see the degradation of the components over time as the condition of the gear worsens. Lastly, the Condition Indicator (CI) is calculated from the EES and the sAES and presented in Figure 12 over the measurement number. It is

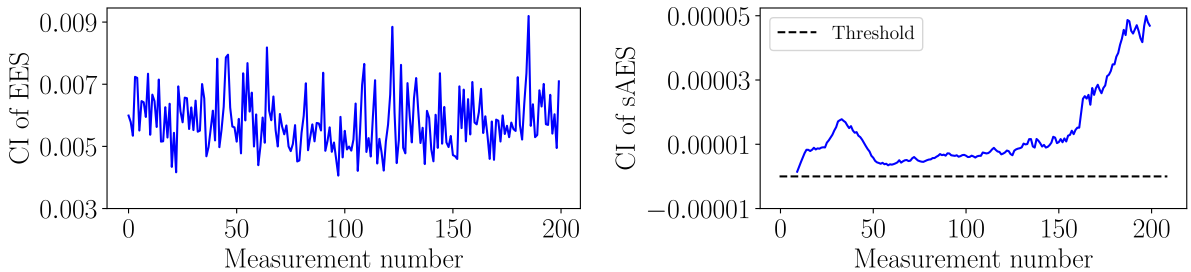

Figure 12: The blind condition indicators of the EES and the sAES are presented over measurement number.

not possible to see the deterioration of the gear in the EES feature, because the signal-to-noise ratios of the damaged components are too low in the EES. This is in contrast to the sAES. The CI associated with the sAES is always larger than zero, which indicates that the system contains anomalous information. Initially the CI makes a hump between the first and the 50th measurements, whereafter the CI steadily increases until the gear failed. We do not know the reason behind the hump in the CI at the start of the experiment, since the gearbox was not opened nor inspected between the start of the measurement and the end of the experiment. However, we speculate that this was due to propagation of the gear damage starting in the initial measurements, whereafter it stabilised until the crack reached its critical length.

Comparing the results against the results obtained with the raw signal in Figure Appendix C, it is evident that the proposed method highlights the fault information in the vibration signal and makes it possible to see the degrading gear component.

4.3. Distributed gear damage experiment

Distributed gear damage modes such as pitting are very frequently encountered in critical rotating machines such as wind turbine gearboxes [26]. The distributed gear damage can result in localised gear damage to develop, which could lead to the failure of the gearbox. Hence, distributed gear damage is also very important to detect, especially under time-varying operating conditions.

The gear of the monitored gearbox was replaced with a healthy gear and tested again. In the healthy and the testing dataset all operating conditions in Figure 7 are considered. Forty measurements were again taken from the healthy gearbox whereafter the gearbox was disassembled and replaced with a different gear that was left in a corrosive environment for a long time. This gear is presented in Figure 13(a), where the surface damage is clearly seen. The damaged gear was tested for approximately eight days before the experiment was stopped due to excessive vibrations that were measured on the gearbox. This damaged gear after the completion of the experiment is presented in Figure 13(b). After inspecting the data, it was observed that the gear experienced a tooth failure at approximately the 100th measurement of the 200 considered in this work, which resulted in the higher loads and impacts on the adjacent teeth. This subsequently resulted in the adjacent gear teeth to fail in the final stages of the test.

The methodology is again similarly applied as in the previous section, where a threshold $\tau(\alpha, f)$ is obtained of the healthy data, which is subsequently used to calculate the AES and the sAES. The 200 measurements that were acquired over the life of the gear are

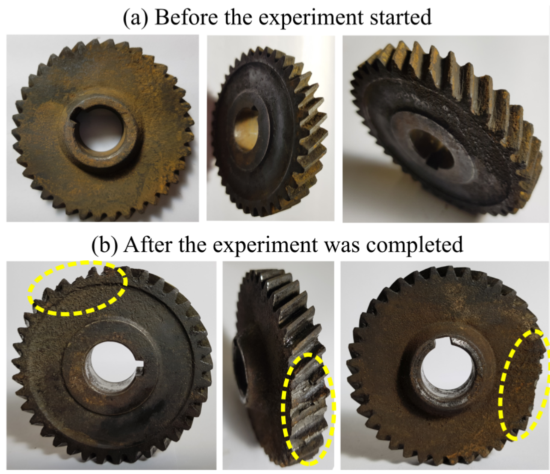

Figure 13: The gear before the experiment started and after the experiment was completed are presented in Figures 13(a) and 13(b) respectively. The damaged regions of the gear are clearly highlighted in Figure 13(b).

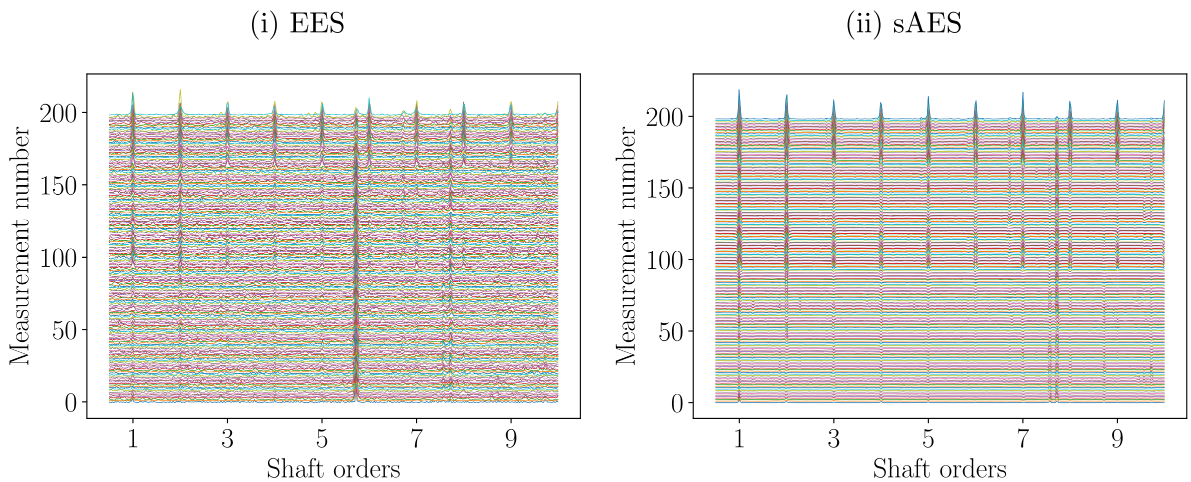

Figure 14: The Enhanced Envelope Spectra (EES) and the smoothed Anomalous Envelope Spectrum (sAES) of the vibration data acquired during the distributed gear damage experiment.

presented in Figure 14 for the EES and the sAES. Both the EES and the SAES are able to detect the gear damage components at 1.0 shaft orders and its harmonics, but the sAES contains much lower noise levels. The benefit of the lower noise levels is highlighted when investigating the condition indicator of the EES and the sAES.

The condition indicators of the EES in Figure 15 contains much noise and it is difficult to detect the deterioration of the gear over time. This is in contrast to the results obtained with the sAES condition indicator that is presented in Figure 15. The CI of the sAES is clearly larger than the threshold, which is indicative that the gearbox contains anomalous behaviour. The changes of the CI of the sAES over time, indicates the degradation of the gear, with the two events associated with the failure of the gear teeth seen at approximately the 100th measurement number and the 175th measurement respectively. Hence, the proposed method results in a significant improvement.

The sAES is therefore very capable of not only detecting that there is damage present

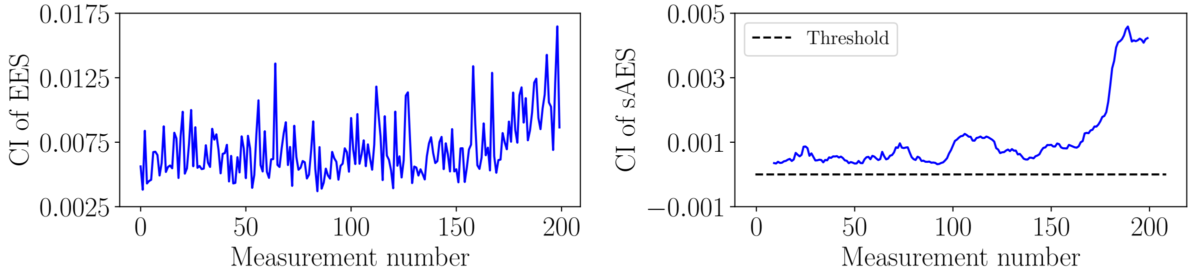

Figure 15: The blind condition indicators calculated with the EES and the sAES are presented over measurement number for the distributed gear damage experiment.

in the system, but it is also possible to determine the cyclic orders of the anomalous component and it is possible to identify when the gearbox is deteriorating over time.

4.4. Healthy gearbox

Vibration data from a healthy gearbox are investigated in this section. This vibration data were not used for estimating the threshold $\tau(\alpha, f)$, i.e. we did not use the training data. The integrated spectra (i.e. EES, AES and sAES) are presented for two measurements of the healthy gearbox in Figure 16. The EES is dominated by the 5.72 shaft orders component. The AES contains spurious anomalous components at different cyclic orders, however, these components are random and are removed in the smoothing process as shown in the sAES. The spurious components are attributed to the vibration data from the gearbox being random and the OFSCoh being very sensitive to weak components.

The condition indicators associated with the EES and the sAES are also presented in Figure 16. The EES contains some random fluctuations, but does not have an increasing trend. In contrast the sAES is 0 for all measurements. This is attributed to the removal of the dominant healthy components by the AES, whereafter the smoothing operation removes the spurious noise components. The results therefore indicate that the proposed method allows us to distinguish between a healthy gearbox and a damaged gearbox.

5. Conclusions and recommendations

A new methodology is proposed in this work to perform fault diagnosis under time-varying operating conditions. This methodology does not require much knowledge about the kinematics of the machine (i.e. it is blind) nor much human effort to interrogate the results. In this methodology, the order-frequency spectral coherence and healthy historical data are used to calculate an anomalous envelope spectrum, a smoothed anomalous envelope spectrum and a condition indicator. These representations can be used for not only detecting damage in the rotating machine, but it can also be used to identify the damaged components and be used to perform fault trending. The methodology is investigated on a numerical gearbox dataset and three experimental datasets, where it is shown that the proposed method has much potential for performing condition monitoring under time-varying operating conditions.

Future work would investigate and compare different methods of modelling the healthy spectral coherences under time-varying operating conditions (e.g. different threshold se-

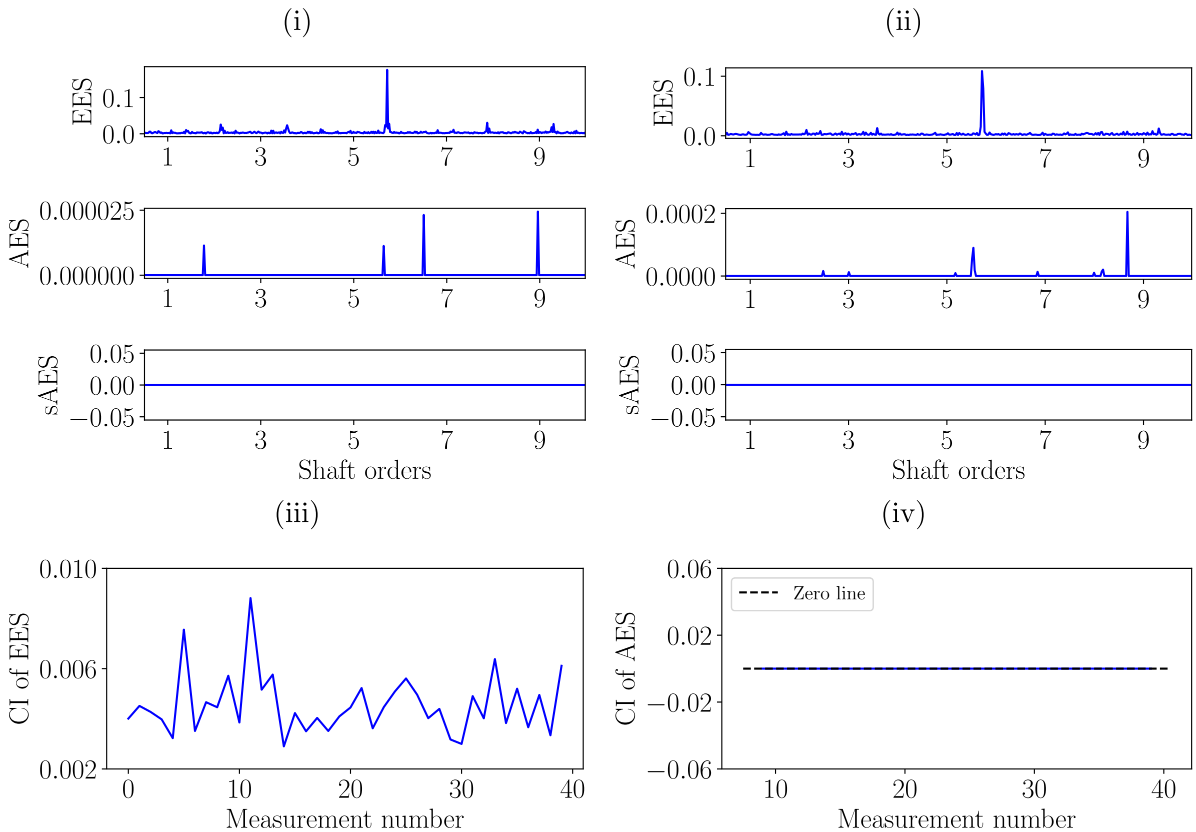

Figure 16: The Enhanced Envelope Spectra (EES) and the smoothed Anomalous Envelope Spectrum (sAES) and their corresponding condition indicators are presented for the vibration data acquired from a healthy gearbox. The healthy gearbox data were acquired from a different experiment compared to the data used in the training procedure.

lection procedures) and also recalibration procedures of the threshold if the gearbox was assembled and disassembled during the monitoring period.

Appendix A. Threshold selection motivation

If the ξth percentile is used in Equation (10) with $\kappa = 1$ there would be $100 - \xi\%$ false positives during monitoring. This would therefore result in regular false alarms and should be avoided. The number of false positives can be reduced by selecting $\kappa > 1$. In general, care should be taken when selecting $\kappa > 1$ as this result in extrapolation. However, this is sensible for this application, because of the following reasons:

- The OFSCoh is very sensitive to weak components and therefore large changes are expected in the OFSCoh if damage is present, i.e. it would exceed the threshold even if $\kappa > 1$.
- The distribution of the OFSCoh is known to be chi-squared distributed [7, 10].

In Figure A.17(i), the false positive rates are presented as a function of κ for different distributions. The probability distribution of the OFSCoh is expected to be chi-squared distributed with two degrees-of-freedom if the length of the signal is very long [7, 10] and it is not expected to be uniform, Gaussian or Laplacian distributed. If $\kappa = 4$, then very few false positives are expected. However, since the OFSCoh is very sensitive to weak damage components, it will still make it possible to detect the damaged components. This is proven by the results in the main document.

Ultimately, the threshold is estimated from a limited number of healthy measurements. This makes the threshold τ a random variable with an underlying sampling distribution. In Figure A.17(ii), the results are presented for the case where we use the 5th and 95th percentile of the sampling distribution of τ as a threshold. The performance of the method is clearly dependent on the number of measurements that are used to estimate the threshold. However, by using $\kappa = 4$ on the OFSCoh data, the results are sufficient for this application.

Appendix B. Phenomenological gearbox model

The model used in this work is based on the model used in Ref. [4]. However, it is important to summarise the signal components for understanding the model. The casing vibration signal of the gearbox with bearing damage can be decomposed as

$$x_c(t) = x_{gmc}(t) + x_{dgd}(t) + x_b(t) + x_n(t), \tag{B.1}$$

The gear mesh component is attributed to the deterministic gear mesh interactions and is calculated with

$$x_{gmc}(t) = M\left(\omega(t)\right) \cdot h_{gmc}(t) \otimes \left(\sum_{k=1}^{N_{gmc}} A_{gmc}^{(k)} \cdot \sin\left(k \cdot N_{teeth} \cdot \int_0^t \omega(\tau) d\tau + \varphi_{gmc}^{(k)} \right) \right), \tag{B.2}$$

where $M\left(\omega(t)\right) = \omega^2$ simulates the dependence of the signal-component to rotational speed. The impulse response function $h_{gmc}(t)$ is approximated with a single degree of

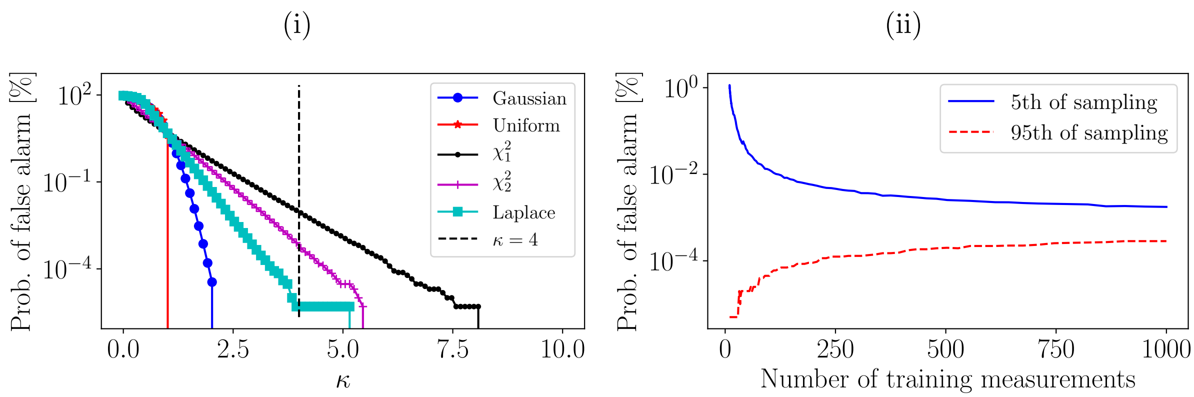

Figure A.17: In Figure A.17(i) the probability of a false alarm is presented for different distributions, calculated using samples from the same distribution as a function of κ in Equation (10). In Figure A.17(ii), the probability of a false alarm is presented for a chi-squared distribution for two degrees of freedom as a function of N using the 5th and 95th percentile of the sampling distribution for calculating the threshold. This illustrates the variance in the results that can be expected when using a limited number of samples for estimating the threshold τ with $\kappa = 4$.

freedom system with a natural frequency of 2000 Hz and a damping ratio of 0.05. The amplitude and phase of the ith gear mesh component are denoted by $A_{gmc}^{(k)}$ and $\varphi_{gmc}^{(k)}$ respectively. The instantaneous gear mesh frequency is calculated with $N_{teeth} \cdot \omega(t)$, where N_{teeth} is the number of teeth on the gear.

The random gear component is attributed to distributed gear damage and is calculated with

$$x_{dgd}(t) = M(\omega(t)) \cdot h_{dgd} \otimes \left(\varepsilon_\sigma(t) \cdot \sum_{k=1}^{N_{dgd}} A_{dgd}^{(k)} \cdot \sin\left(k \cdot \int_0^t \omega(\tau) d\tau + \varphi_{dgd}^{(k)} \right) \right), \tag{B.3}$$

which has the same form as the gear mesh component, except for the additional variable $\varepsilon_\sigma(t)$. The variable $\varepsilon_\sigma(t)$ is sampled from a standardised Gaussian and simulates the interactions between the damaged gear teeth during meshing. The single degree-of-freedom impulse response function of the distributed gear damage component $h_{dgd}(t)$ has a natural frequency of 1300 Hz and a damping ratio of 0.05.

The broadband noise component is calculated with

$$x_n(t) = M(\omega(t)) \cdot \epsilon_\sigma(t) \tag{B.4}$$

which consists of standardised Gaussian noise $\epsilon_\sigma(t)$ being scaled by changes in rotational speed with $M(\omega(t))$.

Bearing damage on the outer race of a rolling element bearing would result in impacts as the rolling elements move in-and-through the defective area. These impacts result in broadband excitation of the structure as it is filtered from the source of the bearing damage through the structure to the transducers. The measured outer race bearing damage signal is simulated with

$$x_b(t) = M(\omega(t)) \cdot h_b(t) \otimes \left(\sum_{k=0}^{N_{imp}-1} A_b^{(k)} \cdot \delta\left(t - T_b^{(k)} \right) \right), \tag{B.5}$$

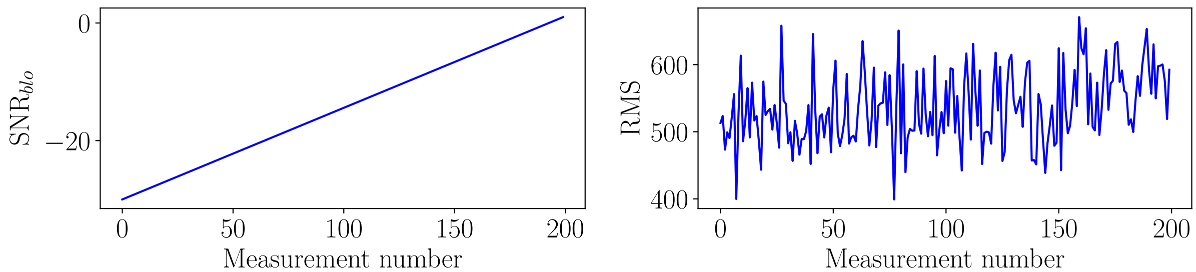

Figure B.18: The signal-to-noise ratio and the Root-Mean-Square (RMS) of the damaged bearing component are presented over measurement number. The signal-to-noise ratio is calculated with $10\log_{10}(E_b/E_n)$ where E_b is the energy of the bearing component and E_n is the energy of the noise component.

where the impulse response function of the bearing damage component $h_b(t)$ has a natural frequency of 7000 Hz and a damping ratio of 0.05. The signal contains N_{imp} impulses, with the kth impulse having a time-of-arrival given by $T_b^{(k)}$ and its magnitude is scaled with $A_b^{(k)}$.

Since it is desired to investigate the ability of the proposed method to perform fault trending the magnitude of the bearing damage component is scaled as shown in Figure B.18. The RMS of the resulting bearing signals are also presented over measurement number.

Appendix C. Experimental results

The root-mean-square of the raw vibration signal; the kurtosis of the raw vibration signal; and the L2/L1 norm ratio of the SES of the raw order tracked signal are presented in Figure C.19. The RMS is very sensitive to time-varying operating conditions and do not clearly indicate that the gear is damaged for the localised gear and distributed gear damage experiment. The kurtosis performs better than the RMS for both cases, but it contains much more noise than the condition indicators obtained with the proposed methodology. The L2/L1 ratio of the SES does not perform well on the considered dataset. Hence, it is clear that the proposed method performs very well in highlighting that the gearbox is damaged and that its health is deteriorating over measurement number.

Acknowledgements

S. Schmidt gratefully acknowledges the Eskom Power Plant Engineering Institute (EPPEI) for their support in the execution of this research.

References

[1] J. Antoni, Cyclostationarity by examples, Mechanical Systems and Signal Processing 23 (4) (2009) 987–1036.

[2] V. Girondin, K. M. Pekpe, H. Morel, J.-P. Cassar, Bearings fault detection in helicopters using frequency readjustment and cyclostationary analysis, Mechanical Systems and Signal Processing 38 (2) (2013) 499–514.

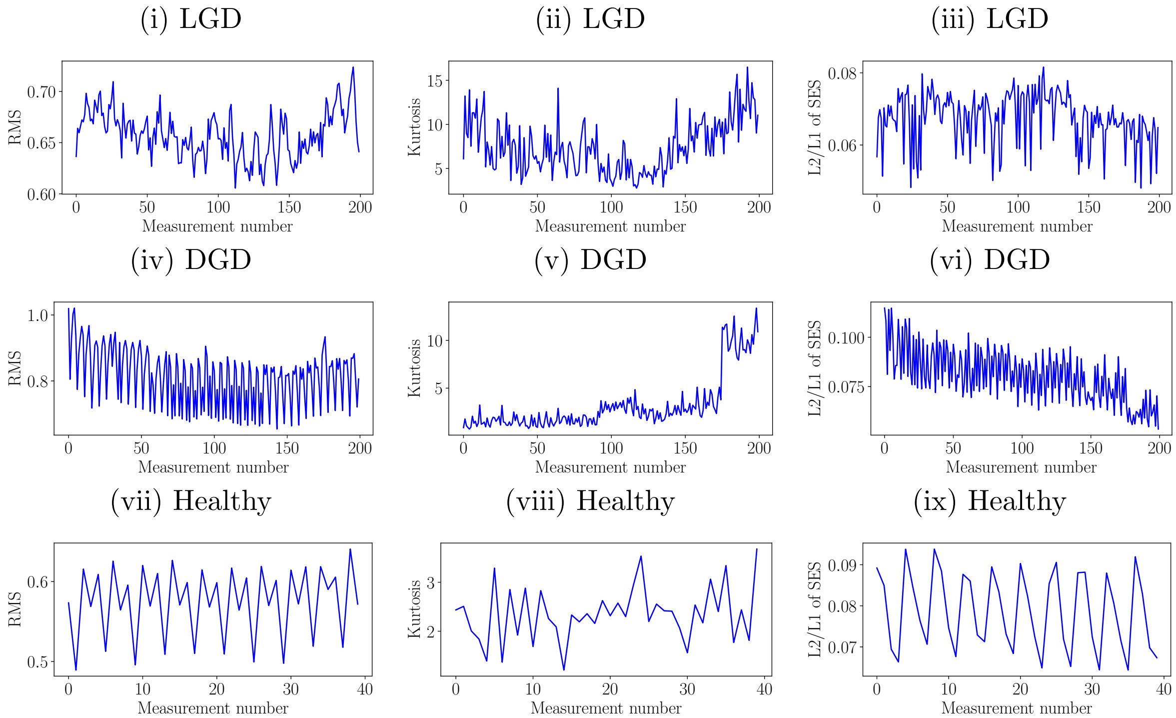

Figure C.19: Three blind metrics are calculated for different experimental signals considered in this work. Abbreviations: Localised Gear Damage (LGD) discussed in Section 4.2; Distributed Gear Damage (DGD) discussed in Section 4.3.

[3] R. B. Randall, J. Antoni, S. Chobsaard, The relationship between spectral correlation and envelope analysis in the diagnostics of bearing faults and other cyclostationary machine signals, Mechanical Systems and Signal Processing 15 (5) (2001) 945–962.

[4] D. Abboud, J. Antoni, S. Sieg-Zieba, M. Eltabach, Envelope analysis of rotating machine vibrations in variable speed conditions: A comprehensive treatment, Mechanical Systems and Signal Processing 84 (2017) 200–226.

[5] J. Urbanek, T. Barszcz, R. Zimroz, J. Antoni, Application of averaged instantaneous power spectrum for diagnostics of machinery operating under non-stationary operational conditions, Measurement 45 (7) (2012) 1782–1791.

[6] N. Baydar, A. Ball, Detection of gear deterioration under varying load conditions by using the instantaneous power spectrum, Mechanical Systems and Signal Processing 14 (6) (2000) 907–921.

[7] J. Antoni, Cyclic spectral analysis in practice, Mechanical Systems and Signal Processing 21 (2007) 597–630.

[8] J. Antoni, Cyclic spectral analysis of rolling-element bearing signals: Facts and fictions, Journal of Sound and Vibration 304 (3-5) (2007) 497–529.

[9] R. Zimroz, W. Bartelmus, T. Barszcz, J. Urbanek, Diagnostics of bearings in presence of strong operating conditions non-stationarity - A procedure of load-dependent

features processing with application to wind turbine bearings, Mechanical Systems and Signal Processing 46 (1) (2014) 16–27.

[10] D. Abboud, S. Baudin, J. Antoni, D. Rémond, M. Eltabach, O. Sauvage, The spectral analysis of cyclo-non-stationary signals, Mechanical Systems and Signal Processing 75 (2016) 280–300.

[11] J. Antoni, G. Xin, N. Hamzaoui, Fast computation of the spectral correlation, Mechanical Systems and Signal Processing 92 (2017) 248–277.

[12] A. Mauricio, J. Qi, W. A. Smith, M. Sarazin, R. B. Randall, K. Janssens, K. Gryllias, Bearing diagnostics under strong electromagnetic interference based on integrated spectral coherence, Mechanical Systems and Signal Processing 140 (2020) 106673.

[13] D. Wang, X. Zhao, L.-L. Kou, Y. Qin, Y. Zhao, K.-L. Tsui, A simple and fast guideline for generating enhanced/squared envelope spectra from spectral coherence for bearing fault diagnosis, Mechanical Systems and Signal Processing 122 (2019) 754–768.

[14] S. Schmidt, P. S. Heyns, K. C. Gryllias, A methodology using the spectral coherence and healthy historical data to perform gearbox fault diagnosis under varying operating conditions, Applied Acoustics 158 (2020) 107038.

[15] F. Jia, Y. Lei, J. Lin, X. Zhou, N. Lu, Deep neural networks: A promising tool for fault characteristic mining and intelligent diagnosis of rotating machinery with massive data, Mechanical Systems and Signal Processing 72-73 (2016) 303–315.

[16] Z. Chen, A. Mauricio, W. Li, K. Gryllias, A deep learning method for bearing fault diagnosis based on cyclic spectral coherence and convolutional neural networks, Mechanical Systems and Signal Processing 140 (2020) 106683.

[17] S. Schmidt, P. S. Heyns, An open set recognition methodology utilising discrepancy analysis for gear diagnostics under varying operating conditions, Mechanical Systems and Signal Processing 119 (2019) 1–22.

[18] Q. Leclère, H. André, J. Antoni, A multi-order probabilistic approach for Instantaneous Angular Speed tracking debriefing of the CMMNO'14 diagnosis contest, Mechanical Systems and Signal Processing 81 (2016) 375–386.

[19] S. Lu, R. Yan, Y. Liu, Q. Wang, Tacholess speed estimation in order tracking: A review with application to rotating machine fault diagnosis, IEEE Transactions on Instrumentation and Measurement 68 (7) (2019) 2315–2332.

[20] P. Borghesani, J. Antoni, A faster algorithm for the calculation of the fast spectral correlation, Mechanical Systems and Signal Processing 111 (2018) 113–118.

[21] R. B. Randall, J. Antoni, Rolling element bearing diagnosticsa tutorial, Mechanical systems and signal processing 25 (2) (2011) 485–520.

[22] W. A. Smith, P. Borghesani, Q. Ni, K. Wang, Z. Peng, Optimal demodulation-band selection for envelope-based diagnostics: A comparative study of traditional and novel tools, Mechanical Systems and Signal Processing 134 (2019) 106303.

[23] A. Mauricio, W. A. Smith, R. B. Randall, J. Antoni, K. Gryllias, Improved envelope spectrum via feature optimisation-gram (iesfogram): A novel tool for rolling element bearing diagnostics under non-stationary operating conditions, Mechanical Systems and Signal Processing 144 (2020) 106891.

[24] D. Wang, Spectral l2/l1 norm: A new perspective for spectral kurtosis for characterizing non-stationary signals, Mechanical Systems and Signal Processing 104 (2018) 290–293.

[25] J. Antoni, The infogram: Entropic evidence of the signature of repetitive transients, Mechanical Systems and Signal Processing 74 (2016) 73–94.

[26] Y. Lin, L. Tu, H. Liu, W. Li, Fault analysis of wind turbines in China, Renewable and Sustainable Energy Reviews 55 (2016) 482–490.